Title
Structure and composition analysis of the phases in the system Th-Pd-B-C containing superconductors with Tc = 14.5 K and Tc = 21 K

Journal
Physica C Superconductivity, 232(3-4)

ISSN
0921-4534

Authors
Zandbergen, HW
Gortenmulder, TJ
Sarrac, JL
et al.

Publication Date
1994-11-01

DOI
10.1016/0921-4534(94)90791-9

ELSEVIER

Physica C 232 (1994) 328–336

PHYSICA C

Structure and composition analysis of the phases in the system Th–Pd–B–C containing superconductors with $T_c = 14.5$ K and $T_c = 21$ K

H.W. Zandbergen [a,*], T.J. Gortenmulder [b], J.L. Sarrac [c], J.C. Harrison [c], M.C. de Andrade [c], J. Hermann [c], S.H. Han [c], Z. Fisk [c], M.B. Maple [c], R.J. Cava [d]

[a] *National Centre for HREM, Laboratory of Materials Science, Delft University of Technology, Rotterdamseweg 137, 2628 AL Delft, The Netherlands*

[b] *Kamerlingh Onnes Laboratory, Leiden University, PO Box 9506, 2300 RA Leiden, The Netherlands*

[c] *Department of Physics and Institute for Pure and Applied Physical Sciences, University of California, San Diego, La Jolla, CA 92093-0319, USA*

[d] *AT&T Bell Laboratories, 600 Mountain Avenue, Murray Hill, NJ 07974, USA*

Received 18 June 1994; revised manuscript received 27 August 1994

Abstract

Several specimens in the system Th–Pd–B–C with nominal compositions $ThPd_3B_2C$ and $ThPd_3B_3C$ (as melted and annealed), containing superconducting phases exhibiting T_c's of 14.5 K and 21 K, have been studied with EPMA, electron diffraction, EDX element analysis and HREM. A number of phases (approximate compositions are given) have been observed: (1) $ThPd_2B_2C$, I-centred tetragonal, $a=0.375$, $c=1.07$ nm, which can be related to the T_c of 14.5 K; (2) $ThPd_{0.65}B_{4.7}$, P-type cubic, $a=0.42$ nm, with a short-range ordered superstructure resulting in diffuse streaks in the electron-diffraction pattern; this phase is suggested to be the 21 K superconducting phase; (3) $ThPd_3$, P-type hexagonal, $a=0.58$, $c=0.98$ nm; (4) $ThPd_8B_3$, I-centred orthorhombic $a=0.84$, $b=0.90$, $c=1.67$ nm; (5) $ThPd_3B_2C$, with unknown structure; (6) ThB_4, tetragonal $a=0.72$, $c=0.41$ nm; (7) graphitic C. Annealing of the specimen $ThPd_3B_2C$ at 1050°C results in the disappearance of $ThPd_2B_2C$ and the loss of the T_c at 14.5 K but a strong increase of the 21 K superconducting fraction with a corresponding strong increase of the phases $ThPd_{0.65}B_{4.7}$ and $ThPd_3$. HREM indicates that $ThPd_{0.65}B_{4.7}$ adopts a modified CaB_6 structure in which the cube face, $\frac{1}{2}$, $\frac{1}{2}$, 0, which is vacant in CaB_6, is partially occupied by Pd with the removal of some B atoms. The superstructure indicates a short-range ordering (clustering) of the Pd atoms.

1. Introduction

Recently quite a number of intermetallic materials containing boron and carbon have been reported to be superconducting [1–3]. Cava et al. have reported superconductivity at 23 K in the system Y–Pd–B–C [1], and a T_c of 16.6 K in the system Lu–Ni–B–C [2]. The superconducting phase in the latter system could be straightforwardly identified as $LuNi_2B_2C$ [2]. $LuNi_2B_2C$ has a fairly simple structure, which is based on the stacking of LuC layers with Ni_2B_2 blocks [4,5] e.g. $(B–Ni_2–B–LuC)_n$. The identification of the 23 K phase in the system Y–Pd–B–C turned out to be difficult. Zandbergen et al. [6] and Fujii et al. [7] have performed electron probe X-ray microanalysis (EPMA), electron diffraction and high-resolution

* Corresponding author.

0921-4534/94/$07.00
SSDI 0921-4534(94)00546-X

electron microscopy (HREM) of several superconducting (T_c=23 K) and non-superconducting specimens in the Y–Pd–B–C system. They concluded that the superconducting phase is YPd_2B_2C having a structure quite similar to that of $LuNi_2B_2C$. Sarrac et al. [3] have reported the presence of two superconducting phases in the system Th–Pd–B–C, one with composition YPd_2B_2C having a T_c of 14.5 K and the $LuNi_2B_2C$ structure [3,8] and one with a T_c of 21 K whose composition and structure are not known. The problem of identifying the 21 K phase in the system Th–Pd–B–C seems to be similar to the identification of the 23 K phase in the system Y–Pd–B–C, since in both cases it is difficult or impossible to synthesize single-phase material.

Similar to the search for the superconducting phase in the system Y–Pd–B–C, we performed an EPMA, electron-diffraction and HREM study of several superconducting (T_c=14.5 K and/or 21 K) in the Th–Pd–B–C system. Seven different phases could be detected. These investigations confirm that the 14.5 K phase is $ThPd_2B_2C$ adopting the $LuNi_2B_2C$ structure, and indicate that the 21 K phase is $ThPd_{0.65}B_{4.7}$.

2. Experimental

The specimens were prepared by mixing elemental Th, Pd, C and B (all 99.9%) in the appropriate proportions and arc melting on a water-cooled copper hearth. Four melts were performed, with the samples turned over between each melt. Samples were then wrapped in Ta foil, placed in an evacuated quartz tube and annealed at 1050°C for several days.

EPMA, electron diffraction and HREM were performed on three samples:

(1) a nominal composition of $ThPd_3B_2C$, with a T_c of 14.5 K with a Meissner fraction of 30% and a very small fraction of the phase with a T_c of 21 K,

(2) a nominal composition of $ThPd_3B_3C$ as melted, containing T_c's of 14.5 K and 21 K both with Meissner fractions of about 2% and

(3) a nominal composition of $ThPd_3B_3C$ annealed at 1050°C for several days, containing no observable fraction of the phase with a T_c of 14.5 K and a 30% Meissner fraction of the phase with a T_c of 21 K. These samples will be coded as 1321, 1331 and 1331a, respectively, in the rest of the paper.

Electron probe X-ray microanalysis (EPMA) was employed for a quantitative assessment of the composition of the various phases present in the three specimens, inhomogeneities in these phases and the fraction of these phases. The specimens were embedded, ground and finally polished using 2.5 μm diamond powder to make them suitable for the EPMA measurements. A Jeol 8621 Superprobe was used, equipped with combined energy dispersive and wavelength dispersive X-ray element analysis systems and JEOL software for instrument control, data acquisition and analysis. Images on a photographic plate were recorded using a 20 keV electron beam energy. The quantitative measurements were performed with 12 keV in the case of Th, Pd and B and 5 keV for C. The beam current was 50 nA. The X-rays of Th Mβ, Pd Lα and B Kα and C Kα are detected with the wavelength dispersive system. A serious handicap is the overlap of the C Kα line (0.277 keV), the only line for C, with the Pd Mz line (0.284 keV). To overcome this problem, the combined lines (C+Pd) were measured and the intensity of the Pd Mz line, determined from the Pd La line was subtracted. As reference materials are used the $ThPd_3$ phase present in sample 1 as Th and Pd standard, pure B and pure C (C lamellae in Fe_3C). The concentrations were calculated using the modified $\Phi(\rho z)$ approach [9].

For the electron-diffraction and HREM experiments, thin specimens were obtained by crushing under ethanol and mounting the crystal fragments on a Cu grid covered with a carbon coated holey film. In general this method results in particles ranging in size from 0.05 to 5 μm, which are often single phase. Electron microscopy was performed with a Philips CM30ST electron microscope with a field emission gun and a Philips CM30T, both operating at 300 kV and equipped with a Link EDX element analysis system.

Image calculations were carried out for several models using a MacTempas software program, in which the following parameters were used: Cs=1.3 mm, defocus spread 5 nm, objective aperture 10 nm^{-1}, beam convergence 0.1 mrad, and mechanical vibration 0.03 nm. The thickness and defocus were varied.

3. Experimental results

3.1. EPMA, EDX and electron diffraction

EPMA shows that the three specimens contain a large number of phases, which are listed in Table 1. Backscattered electron images of the three specimens are shown in Fig. 1. Most phases are clearly distinguishable in the backscattered electron images, due to their different gray levels, but the phases A3 and A6 ($ThPd_3$ and ThB_4) have almost the same appearance. They could be distinguished by using Pd element mapping, since ThB_4 does not contain any Pd whereas it is the major component in $ThPd_3$. Also the phases A1 ($ThPd_2B_2C$) and A2 ($ThPd_{0.65}B_{4.7}$) are difficult to distinguish.

The unit cells and the Th/Pd ratios of many crystal fragments were determined by electron diffraction and EDX element analysis. The phases which could be detected in the various specimens are given in Table 1. Electron-diffraction patterns of some of the phases are given in Fig. 2.

It was observed that the fraction of the C-like phase was higher in the electron-microscopy study than in the backscattered electron images. This is probably due to the non-representative sampling in the preparation of the specimens for the electron-microscope study. Because of the low density of this phase it is quite likely that it remains longer in dispersion in the ethanol used to deposit the particles on the carbon film coated Cu grid.

The plate-like phase (A1) is only present in the specimens 1321 and 1331. The composition is determined by EPMA to be $ThPd_2B_2C$. The structure as determined by HREM [8] indicates that this phase adopts the $LuNi_2B_2C$ structure; it is schematically presented in Fig. 3. A [100] diffraction pattern is given in Fig. 2(a). The plate-like morphology is similar to the shapes of the crystals of $LuNi_2B_2C$ [10] and YPd_2B_2C [6].

The backscattered electron image of specimen 1331a shows the plate-like remnant of $ThPd_2B_2C$ which was decomposed during the annealing at 1050°C. The EPMA measurements indicate that $ThPd_2B_2C$ is decomposed in three phases: A3 ($ThPd_3$), A2 ($ThPd_{0.65}B_{4.7}$) and a C-rich phase. The C-rich phase is probably pure C, since with electron diffraction no other structures than those of $ThPd_3$, $ThPd_{0.65}B_{4.7}$, and graphitic C are observed in specimen 1331a.

Diffraction patterns of $ThPd_{0.65}B_{4.7}$ (A2), are shown in Figs. 2(b) and (c), indicating a primitive cubic unit cell with $a=0.415$ nm. EPMA indicates a composition $ThPd_xB_y$ with x between 0.65 and 0.7

Table 1
The phases observed by EPMA, EDX and electron diffraction (h=high, i=intermediate, l=low, a=absent)

Code	Morphology from EPMA	Structural data from electron diffraction	Element ratios according to				Suggested phase	Specimen		
			EPMA			EDX Pd/Th		1321	1331	1331a
			Pd/Th	B/Th	C/Th					
A1	Plates	Tetr., $a=0.38$, $c=1.07$	2	1.9–2.2	1	2	$ThPd_2B_2C$	h/h	i/i	a/a
A2	Rounded facets	Cubic, $a=0.42$, superstructure	0.65–0.7	4–5	0	0.6–0.7	$ThPd_{0.65}B_{4.7}$	l/l	a/i	h/h
A3	Sharp facets	Hexagonal, $a=0.58$, $c=0.97$	3	0	0	3	$ThPd_3$	i/i	i/i	h/h
A4	Matrix	Ort, I-cent, $a=8.4$, $b=9.0$, $c=1.67$	6–9	2–3	0	6–8	$ThPd_8B_3$	h/i	l/a	a/a
A5	Facets	Unknown	3	2–2.2	1	?	$ThPd_3B_2C$	a/?	a/?	l/?
A6	Rounded facets	Tetrag. $a=0.72$ $c=0.41$	4–5	0	0	4	ThB_4	a/a	i/h	a/a
A7	Spheres	Hexagonal, graphite-like	–[a]	–[a]	high	–[a,b]	C	l/–[b]	l/–[b]	a/–[b]
A8	Plate-like	Hexagonal, graphite-like	–[a]	–[a]	high	–[a]	C	a/l[b]	i/h[b]	i/h[b]
A9	Lamellae	?	–[a]	–[a]	high	–[a]	C	a/–[b]	a/–[b]	i/–[b]

[a] Large variations occur in the Th, Pd and B content due to the presence of small particles of the other phases in the C matrix.
[b] Electron diffraction does not allow for a distinction between the phases A7, A8 and A9; therefore all data are given for A8. A7 is also known to be graphite-like because this phase is the only C compound in specimen 1321, in which electron diffraction shows the presence of a graphite-like phase.

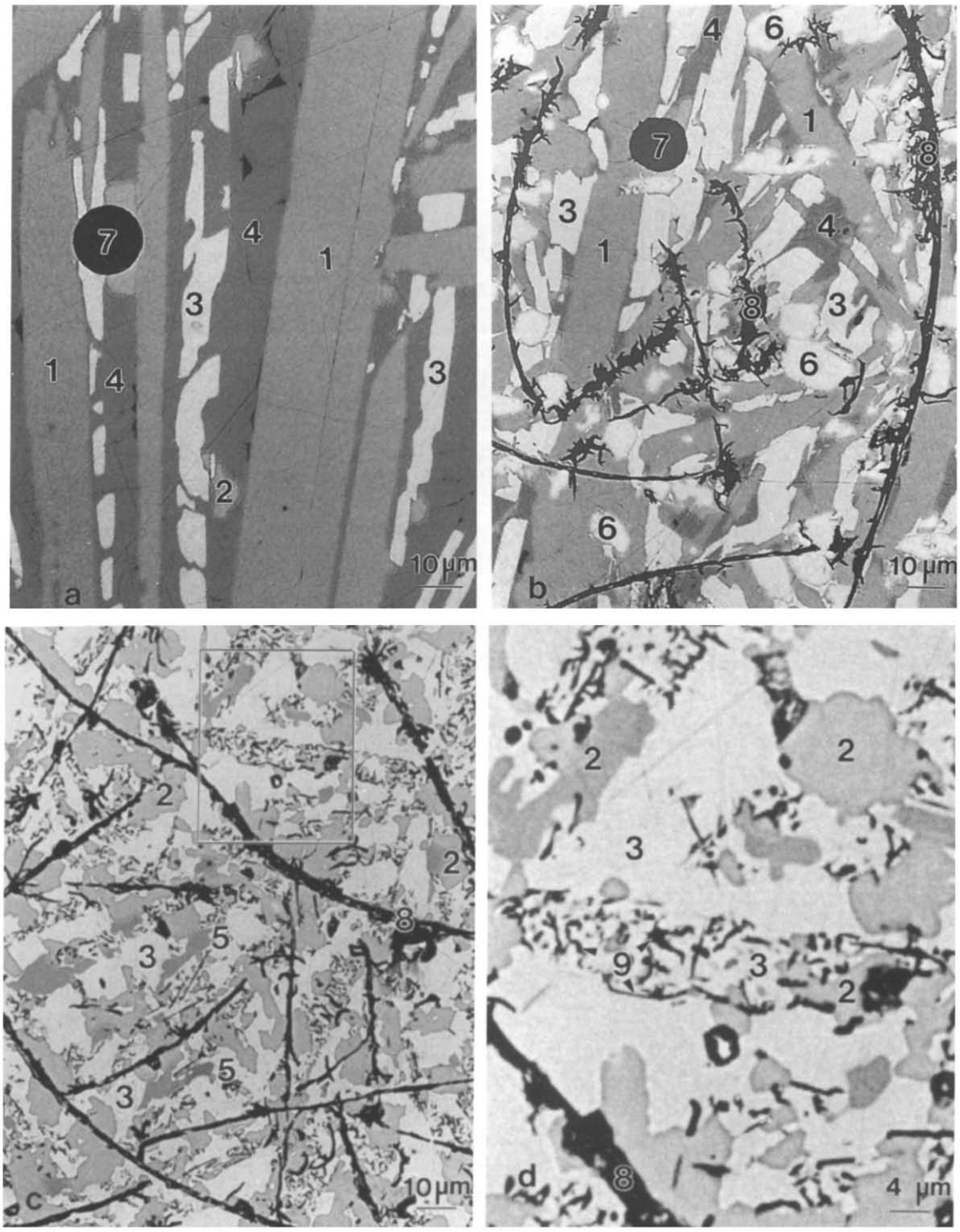

Fig. 1. Backscattered electron images. (a) The specimen with a nominal composition $ThPd_3B_2C$ having a 30% Meissner fraction of the $T_c = 14.5$ K phase. (b) The specimen with a nominal composition $ThPd_3B_2C$ having T_c's of 14.5 and 21 K (2% Meissner fractions). (c) As (b) but annealed at 1050°C showing only a T_c of 21 K (30% Meissner fraction). (d) Enlargement of boxed area in (c). The numbers in the figures refer to the codes for the phases listed in Table 1.

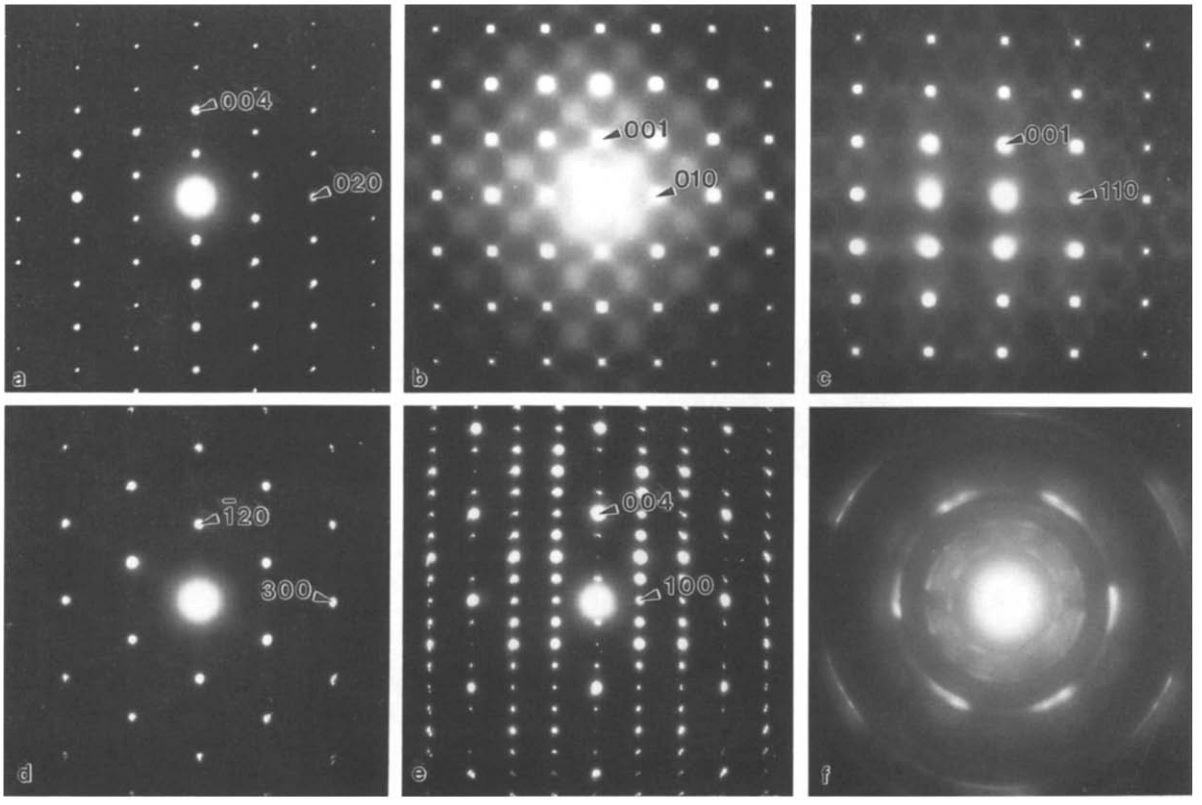

Fig. 2. Diffraction patterns of several phases observed. (a) shows a [100] diffraction pattern of $ThPd_2B_2C$ (A1). (b) and (c) show [100] and [1$\bar{1}$0] diffraction patterns of the cubic phase (A2); diffuse scattering can be observed in both diffraction patterns. (d) and (e) show the [001] and [100] diffraction patterns of $ThPd_3$ (A3). (f) shows an example of a diffraction pattern of the C-rich phase.

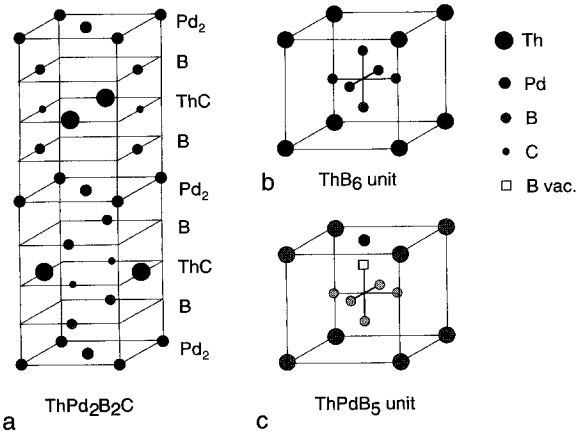

Fig. 3. Schematic representation of the structures of (a) $ThPd_2B_2C$, (b) the structure of ThB_6, (c) the $ThPdB_5$ structure unit with a vacancy on one of the B sites.

and y between 4 and 5.5. For reasons given in Section 4 the composition is written as $ThPd_{0.65}B_{4.7}$. All crystals show the presence of a superstructure, which is reflected in a rather complicated diffuse scattering as can be seen from Figs. 2(b) and (c). The diffuse scattering indicates that the superstructure is only short-range ordered. The large abundancy of this phase and its small and very small volume fraction in the specimens 1321 and 1331, respectively, suggest that this phase is the 21 K superconducting phase.

According to the EPMA measurements the phase $ThPd_3$ (A3) is present in all three specimens with a fraction of at least 10%. Electron diffraction (see Figs. 2(d) and (e)) shows that this phase has a hexagonal unit cell with $a=0.58$, $c=0.95$ nm with $00l$, $l\neq 4n$, absent which is in agreement with the structure reported for $ThPd_3$ by Thom et al. [11]. Since this phase is present in the specimens 1321 and 1331 with a fairly large volume fraction ($>15\%$) it is very un-

likely that this phase is the 21 K superconductor.

The various diffraction patterns of phase A4 could be indexed with an I-centred orthorhombic unit cell with $a=0.84$, $b=0.90$ and $c=1.67$ nm with the approximate composition $ThPd_8B_3$. In the Y–Pd–B system, a phase with the same composition and unit cell has been found [6].

We attempted to obtain diffraction information from the phase $ThPd_3B_2C$ (A5). Since only the Pd and Th and not the B or C content can be measured by the EDX equipment used, about 100 particles having a Pd/Th ratio of 3 were selected. All these particles showed diffraction patterns of $ThPd_3$. Either $ThPd_3B_2C$ has a structure similar to that of $ThPd_3$, or none of the crystals investigated were of the intended phase.

The diffraction patterns of phase A6 indicate a P-type tetragonal unit cell with $a=0.72$, $b=0.41$ nm. This unit cell and the absence of Pd indicate that this phase is ThB_4 [8].

The two main carbon-rich phases are present as large spherical particles (A7) or platelets (A8) scattered randomly. A typical diffraction pattern is shown in Fig. 3(f), showing rings; the positions of these rings are compatible with graphitic C. In addition to this, some C-rich particles are observed in the backscattered electron images at the decomposed $ThPd_2B_2C$ regions in specimen 1331a. The structural nature of these particles could not be detected, because, due to the sample preparation (crushing) for the electron-diffraction investigation, the correlation with the location in the specimen is lost. However, we observed no evidence that this C-rich phase is different from graphitic C.

3.2. High-resolution electron microscopy

A HREM study of $ThPd_2B_2C$ has been reported previously [8]. It showed that $ThPd_2B_2C$ adopts a $LuNi_2B_2C$-like structure, possibly with a deficiency in B. No planar stacking defects could be observed, indicating a strict layer sequence $\{B–Pd_2–B–ThC\}_n$. At the edge of wedge-shaped crystals the $ThPd_2B_2C$ lattice transforms into a cubic-like structure with $a=0.41$ nm during the HREM investigation, an example of which is given in Fig. 4. This cubic-like structure is face centred cubic and is consequently different from that of $ThPd_{0.7}B_{4.6}$. We have reported previously [6] that the YPd_2B_2C lattice also changes into this cubic-like structure by the interaction of the electron beam.

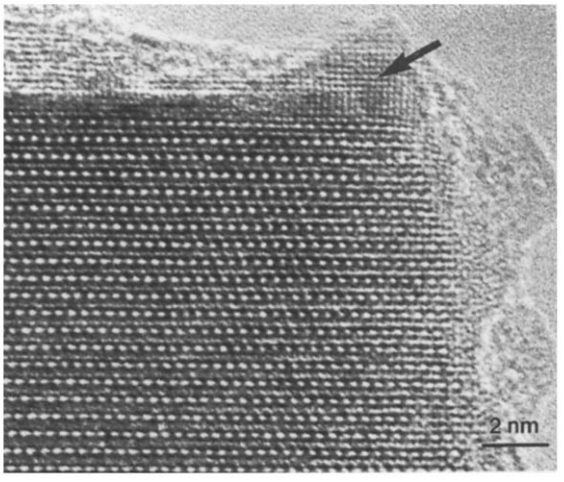

Fig. 4. [100] HREM image of $ThPd_2B_2C$ in which the Th and Pd atoms are imaged as bright dots. A calculated image is shown as inset. The cubic phase due to electron-beam induced decomposition is indicated by the arrow.

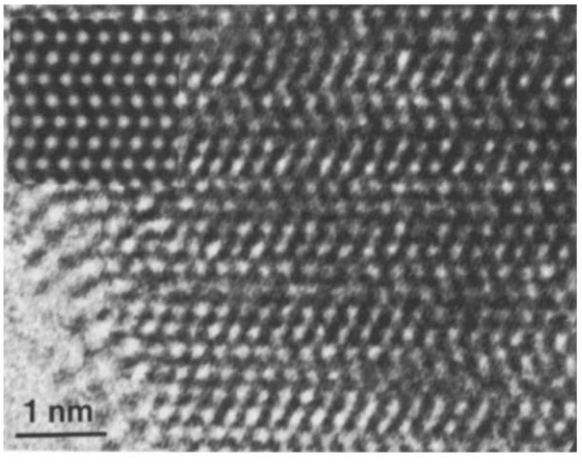

Fig. 5. [100] HREM image of YPd_3 in which the Th and Pd atoms are imaged as bright dots. A calculated image (thickness 2 nm, defocus −80 nm) is shown as inset.

HREM on $ThPd_3$ showed that the structure as reported for $ThPd_3$ [11] is adapted. An experimental image and matching calculated image is shown in Fig. 5. It was observed that the structure near the surface was modified when the specimen was exposed to air, making it rather difficult to obtain HREM images of the bulk structure.

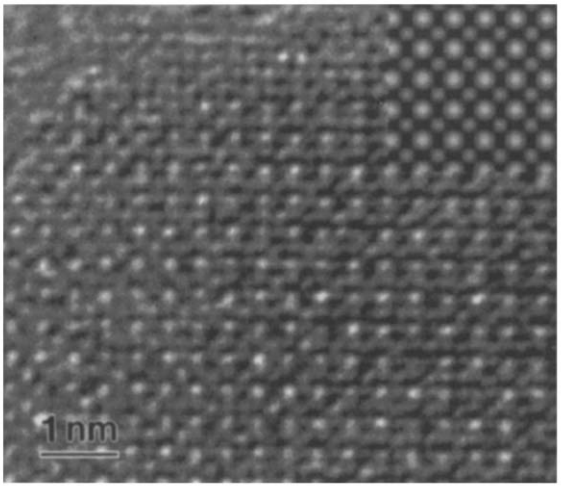

Fig. 6. [100] HREM image of $ThPd_{0.65}B_{4.7}$ in which Th is imaged as the large white dot and the Pd atom at 0, $\frac{1}{2}$, 0 $\frac{1}{2}$ as the small white dot. A calculated image (thickness 2 nm, defocus −80 nm) is shown as inset.

HREM on $ThPd_{0.65}B_{4.7}$ shows that this compound has simple HREM images, which can be explained with a cubic structure in which a very strongly scattering atom (Th) occupies the position 0, 0, 0 and a much less scattering atom the position $\frac{1}{2}$, $\frac{1}{2}$, 0 as indicated in Fig. 3(c); the superstructure is not visible in these images, which is logical if one considers that the superstructure is very weak. Fig. 6 shows an experimental [100] image and the corresponding calculated image. For the calculation a model was used which is based on the CaB_6 structure, in which Ca (position 0, 0, 0) is replaced by Th and Pd is located on the position $\frac{1}{2}$, $\frac{1}{2}$, 0 with an occupancy of 0.22. Due to this Pd some B atoms have to be removed. This results in: Th at 0, 0, 0 with full occupancy, Pd at $\frac{1}{2}$, $\frac{1}{2}$, 0 with 0.22 occupancy and B on 0.21, $\frac{1}{2}$, $\frac{1}{2}$ with an occupancy of 0.78. Because of the low scattering cross-section of B the effect of presence or absence of B is small and cannot be distinguished based on fits with the experimental image. A detailed study of this structure will be presented elsewhere [12].

4. Discussion

In principle, all phases which remained or grew during the annealing at 1050°C could be the 21 K superconducting phase. Evidently $ThPd_2B_2C$ is destroyed by the annealing and cannot be correlated to the T_c of 21 K. The only two phases which grow substantially during the annealing are $ThPd_3$ and $ThPd_{0.65}B_{4.7}$. Furthermore a small volume fraction (< 5%) of $ThPd_3B_2C$ is formed. The volume fraction of the latter one is insufficient to explain the observed Meissner fraction in the 1331a specimen. The Meissner fraction of about 30% can only be explained assuming $ThPd_3$ or $ThPd_{0.65}B_{4.7}$ to be the superconductor. Since $ThPd_3$ is also present with a volume fraction of about 15% or more in the specimen 1321, which shows hardly any superconductivity at 21 K, it can be concluded that this phase is not the superconductor. Furthermore the C plates occur with the same volume fraction in specimens 1331 and 1331a, which cannot account for the large difference in Meisner fraction of these specimens. Consequently the 21 K superconductor must be the phase $ThPd_{0.65}B_{4.7}$.

It is concluded that $ThPd_2B_2C$ is the phase with a T_c of 14.5 K because of the following reasons:

(1) the specimen 1321 contains more than 40% of this phase and shows a 14.5 K Meissner fraction of about 30%;

(2) this phase is absent in the specimen 1331a which shows no superconducting transition at 14.5 K;

(3) the structure as determined by HREM [8] indicates that this phase adopts the $LuNi_2B_2C$ structure, a structure which has shown superconductivity for many analogous compounds. The plate-like morphology of $ThPd_2B_2C$ is similar to the shapes of the crystals of $LuNi_2B_2C$ [10] and YPd_2B_2C [6]. Since it consists of extended plates, it can easily form an interconnecting network allowing zero resistance and the large magnetic screening below T_c. In the 1050°C annealed specimen only the remnant of these plates can be observed, which contain $ThPd_3$, $ThPd_{0.65}B_{4.7}$ and C.

Electron-beam induced surface changes are observed for $ThPd_2B_2C$ (Fig. 4) leading to a cubic-like structure with an a-axis of about 0.41 nm, suggesting the formation of an F-centred cubic unit cell ($ThPd_2$ without any ordering of Th and Pd and with some B and C at interstitial positions) due to loss of C and B. Apart from this surface change, another change occurs in the structure of $ThPd_2B_2C$ itself: a decrease

of the c-axis when irradiated by the electron beam of about 0.3 nm. Such a decrease is also observed for $ThPd_2B_2C$ and $ThPd_2B_2C$ but in those compounds the decrease is larger, e.g. 0.06 nm. The reason for this decrease is not yet understood.

All phases observed by EPMA can be correlated to the phases observed by electron diffraction and EDX analysis as is evident from Table 1. Some differences in the volume fractions as observed by EPMA and TEM do occur. Partly this can be explained by the non-representative sampling by TEM caused by the preparation method (C phase). The difference in the fraction of $ThPd_{0.65}B_{4.7}$ (not observed by EPMA) might be due to a non-random distribution of this phase over the melted button.

The B and C compositions can only be determined from the EPMA measurements. The accuracy of the element analysis by EPMA is quite high for the elements Th and Pd (better than a few % for Th/Pd ratio) but rather low for the elements B and C (about 20% and 40% accuracies, respectively) because of their extremely low X-ray yield and large absorption corrections. The C content contains an extra uncertainty because of the overlap of this X-ray peak with an X-ray peak of Pd. The uncertainty in the contents of these elements is for instance reflected in the composition of ThB_4 which in fact is measured by EPMA as approximately ThB_5. This implies that the exact B composition of the 21 K phase, $ThPd_{0.65}B_{4.7}$, is not accurately known.

HREM shows that $ThPd_{0.65}B_{4.7}$ adopts a cubic structure with a heavy scattering atom on the cube corners and a lesser scattering atom in the faces of the cube. Given the Th/Pd ratio the most likely structure is the one depicted in Fig. 3. Image calculations with this model give a good fit with the experimental image. The presence of Pd on 0.22 of the cube faces must result in a restriction of the number of B atoms because of the too short Pd–B distance. Omitting these B atoms results in a composition $ThPd_xB_{6-2x}$, giving with $x=0.65$ $ThPd_{0.65}B_{4.7}$, which is in good agreement with the composition determined by EPMA. Carbon is not necessary for the structure, but it could be an essential addition to obtain superconductivity. The EPMA measurements indicate that if carbon is present in the structure it is only for a few atomic percent.

The CaB_6 structure is reported for several superconductors. For instance, ThB_6 [13] is reported to have a T_c of 0.78 K, whereas Matthias et al. [14] report a T_c about 7 K for YB_6. This indicates that the CaB_6 structure is in principle a structure allowing for a relatively high superconductivity. We have prepared specimens with the nominal composition $ThPd_{0.65}B_{4.7}$. These specimens, however, showed to be far from single phase and showed a considerably lower superconducting fraction. This indicates that the chemistry of this system is complicated, in analogy to the system Y–Pd–B–C in which the superconducting phase can only be prepared in a small composition window far from the actual composition of the superconductor YPd_2B_2C.

The origin of the superstructure of $ThPd_{0.65}B_{4.7}$ must be very short-range order, since the superstructure results only in a diffuse intensity in the diffraction patterns. Most probably it is caused by the ordering of the Pd atoms.

The structure of $ThPd_{0.65}B_{4.7}$ might be similar to that of $YPd_{1.2}B_{3.3}$ [6], which also has a cubic unit cell with $a=0.42$ nm, but with sharp superstructure reflections, indicating long-range order. In the case of similar structure the composition of $ThPd_{1.2}B_{3.3}$ should be $ThPd_{1.2}B_{3.6}$ because of the composition formula YPd_xB_{6-2x}.

It is intriguing that also in the system Y–Pd–B–C a phase with a structure similar to that of $ThPd_{0.65}B_{4.7}$ is present: $YPd_{1.2}B_{3.3}$ [6], which also has a cubic unit cell with $a=0.42$ nm, but with sharp superstructure reflections, indicating long-range order. This leads to the question whether the 23 K superconductor in the system Y–Pd–B–C is indeed $ThPd_2B_2C$ or $YPd_{1.2}B_{3.3}$, the more because both phases decompose upon annealing at 800°C.

With respect to the preparation of a pure phase there is an important difference between the 21 K superconductor in the system Th–Pd–B–C and the 23 K superconductor in the system Y–Pd–B–C. Whereas the 23 K superconductor decomposes upon annealing at 800°C, the 21 K superconductor, $ThPd_{0.65}B_{4.7}$, is stable upon annealing even at 1050°C. The increase of $ThPd_{0.65}B_{4.7}$ upon annealing indicates that this phase can in principle be made as a single phase, provided the diffusion rate of all atoms is sufficiently high.

5. Conclusion

Detailed analysis of the phases in the various specimens in the Th–Pd–B–C system indicates that the 14.5 K superconducting phase is $ThPd_2B_2C$ and that the 21 K superconductor is $ThPd_{0.65}B_{4.7}$. $ThPd_2B_2C$ has a structure similar to that of $LuNi_2B_2C$. $ThPd_{0.65}B_{4.7}$ adopts a cubic structure with Th on the corners and Pd with a partial occupancy in the faces of the cube. Local ordering of the Pd vacancies results in a short-range superstructure.

Acknowledgements

Two of the authors (HWZ and TJG) wish to thank the Foundation for Fundamental Research on Matter and the Netherlands Technology Foundation for support. Work at UCSD was supported in part by the U.S. Department of Energy under Grant No. DE-FC03-86ER45230. Financial support of the CNPq of Brasil (MCA) and of the German Academic Exchange Service (JH) is gratefully acknowledged.

References

[1] R.J. Cava, H. Takagi, B. Batlogg, H.W. Zandbergen, J.J. Krajewski, W.F. Peck Jr., R.B. van Dover, R.J. Felder, T. Siegrist, K. Mizuhashi, J.O. Lee, H. Eisaki, S.A. Carter and S. Uchida, Nature (London) 367 (1994) 148.
[2] R.J. Cava, H. Takagi, H.W. Zandbergen, J.J. Krajewski, W.F. Peck Jr., T. Siegrist, R.B. van Dover, R.J. Felder, K. Mizuhashi, J.O. Lee, H. Eisaki and S. Uchida, Nature (London) 367 (1994) 252.
[3] J.C. Sarrac, M.C. de Andrade, J. Hermann, S.H. Han, Z. Fisk, M.B. Maple and R.J. Cava, Physica C 229 (1994) 65.
[4] T. Siegrist, H.W. Zandbergen, R.J. Cava, J.J. Krajewski and W.F. Peck Jr., Nature (London) 367 (1994) 254.
[5] H.W. Zandbergen, R.J. Cava, J.J. Krajewski and W.F. Peck Jr., Physica C 224 (1994) 6.
[6] H.W. Zandbergen, W.G. Sloof, R.J. Cava, J.J. Krajewski and W.F. Peck Jr., Physica C 226 (1994) 365.
[7] H. Fujii, S. Ikeda, S.I. Arisawa, K. Hirata, H. Kumakura, K. Kadowaki and K. Togano, Jpn. J. Appl. Phys. Lett., to be published.
[8] H.W. Zandbergen, E.J. van Zwet, J.C. Sarrac, M.C. de Andrade, J. Hermann, S.H. Han, Z. Fisk, M.B. Maple and R.J. Cava, Physica C 229 (1994) 29.
[9] G.F. Bastin, H.J.M. Heijligers and F.J.J. van Loo, Scanning 8 (1986) 45.
[10] H.W. Zandbergen, W.G. Sloof, R.J. Cava, J.J. Krajewski and W.F. Peck Jr., Physica C 226 (1994) 365.
[11] Thom et al., Adv. X-ray Anal. 62 (1962) 91.
[12] H.W. Zandbergen, E.J. van Zwet, J. Jansen, J.C. Sarrac, Z. Fisk, M.B. Maple and R.J. Cava, Philos. Mag. Lett., submitted.
[13] Zalki et al., Acta Crystallogr. 6 (1953) 269.
[14] Matthias et al., Phys. Rev. B 11 (1969) 1866.